JOURNAL OF MATERIALS SCIENCE 21 (1986) 2557–2564

Phase decompositions of Fe–Si–Al ordered alloys

TORU MIYAZAKI, TAKAO KOZAKAI, TAKESHI TSUZUKI*
Department of Materials Science and Engineering, Metals Section, Nagoya Institute of Technology, Gokiso-cho, Showa-ku, Nagoya, 466, Japan

Stable structures of Fe–Si–Al ternary alloys and Fe–Si and Fe–Al binary alloys containing up to about 40 at% solute atoms were investigated by means of transmission electron microscopy. The following results were obtained. Two types of phase separation, B2 + DO_3 and α + DO_3 were observed in the alloys whose compositions lie in a narrow band connecting Fe–10 to 14 at% Si with Fe–20 to 25 at% Al and also in the neighbourhood of a Fe–30 at% Al–3 at% Si alloy. Such compositions of the alloys are located in the phase boundary of B2 and DO_3 single phases or α and DO_3 single phases. The phase separation in the Fe–Si–Al and Fe–Si alloys produce the ⟨1 0 0⟩ modulated structure which differs from the morphology formed by the phase separation of the Fe–Al system.

1. Introduction

To date, investigations on the phase decompositions of super saturated solid solutions have mainly been performed for the alloy systems having a positive interaction energy between the nearest neighbour atoms. Recently, however, phase seaparations in the ordered solid solutions have experimentally been found in several alloys such as Cu–Mn–Al [1], Cu–Zn [2, 3], Fe–Al [4, 9], Fe–Si [10–13] and so on. Theoretical pursuits of this phenomenon have also been conducted [14–19], which are essentially based upon taking into account the interatomic interactions not only between the nearest neighbour atoms but also the second and the higher order neighbours. In theoretical treatments of this sort, even if the first order interaction energy is negative, phase decompositons are expected to occur when the second and the higher order interaction energies are positive.

Phase decompositions of the Fe–Si alloys, one of the typical ordered alloys, were first examined by Warlimont [20] who found a coexistence of two ordered phases. Thereafter, Inden and co-workers [14–18] theoretically led a phase diagram showing coexistence of B2 (FeSi) and DO_3 (Fe_3Si) ordered phases in the composition range 10 to 13 at% Si on the basis of free energies theoretically evaluated by introducing four sublattices which can represent the DO_3 superlattice, three kinds of ordering parameter, first and second neighbour interaction energies and a magnetic parameter of iron atoms. Paider [19] calculated the spinodal line of this phase decomposition.

The phase separation (B2 + DO_3) was also recognized experimentally by means of neutron diffraction [10], specific heat measurement [11] and transmission electron microscopy [12, 13]. Recently, Kubo [21] proposed kinetic equations of this phase separation based on a so-called descrete lattice model developed by de Fontaine [22]. As mentioned above, the phase separation of the Fe–Si binary system is considered to have almost been settled.

On the Fe–Al binary alloy which is also a typical ordered system, two types of phase separation, α + B2 and α + DO_3, have been found experimentally and theoretically by Allen and co-worker [5, 23], Oki *et al.* [8, 9] and Swann *et al.* [6, 7]. Furthermore, recently Hasaka and Ikeda [24] predicted a coexistence of B2 and DO_3 phases in the composition range over 30 at % Al.

As mentioned above, the phase separations in Fe–Si and Fe–Al binary systems have already become clear. However, investigations on phase separations of the Fe–Si–Al ternary system have not been found, so far as we know. The Fe–Si, Fe–Al and Fe–Si–Al systems contain several industrially important alloys such as the silicon steel, Alfel alloy, Sendust alloy and the low magnetic strain alloy, which has recently gained attention (e.g. [25]). Therefore, it is considered valuable to elucidate the phase transformations of this ternary system.

The aim of this paper is to show microstructural changes with ageing of iron-rich Fe–Si–Al ordered ternary alloys by means of transmission electron microscopy, and to propose phase diagrams of the ternary system.

2. Specimens and experimental procedures

Many Fe–Si, Fe–Al and Fe–Si–Al alloys, whose chemical compositions are summarized in Table I, were prepared from 99.98% at % Fe, 98.6 at % Si and 99.99 at % Al in a vacuum induction furnace. Most of these alloys were forged and rolled at high temperature (1400 to 1500 K) to a thin plate of 0.4 mm thickness. These specimens were homogenized at tem-

Present address: Nippon Steel Co Ltd, Nagoya Works, Japan.

0022–2461/86 $03.00 + .12

TABLE I Chemical compositions of specimens and solution-treatment temperatures

Alloy	Si(at %)	Al(at %)	ST temperature (K)
S-1	10.9	–	1473
S-2	13.0	–	1473
S-3	20.5	–	LQ
S-4	27.7	–	LQ
A-1	–	28.1	LQ
A-2	–	31.4	LQ
A-3	–	33.2	LQ
SA-1	10.9	0.5	1323
SA-2	10.9	1.1	1323
SA-3	10.8	2.0	1423
SA-4	10.5	3.8	1523
SA-5	9.9	7.5	1673
SA-6	8.2	1.4	1273
SA-7	8.1	3.2	1523
SA-8	7.7	6.6	1573
SA-9	6.6	12.3	1673
SA-10	5.8	2.9	1273
SA-11	5.5	6.3	1473
SA-12	5.0	9.0	1573
SA-13	3.0	9.4	1173
SA-14	2.8	12.1	1273
SA-15	2.7	17.7	1673
AS-1	5.0	23.7	LQ
AS-2	10.0	22.5	LQ
AS-3	15.1	21.2	LQ
AS-4	3.0	29.9	LQ
AS-5	3.0	33.0	LQ

peratures shown in Table I for 1 h, and then drop-quenched into iced brine. The alloys shown as LQ in the solution treatment (ST) temperature column in Table I were directly quenched from the melt by means of a so-called single roller technique instead of the usual solution treatment, because these alloys were too brittle to be forged even at high temperatures. The ribbon-specimens were about 30 μm thick. All of the

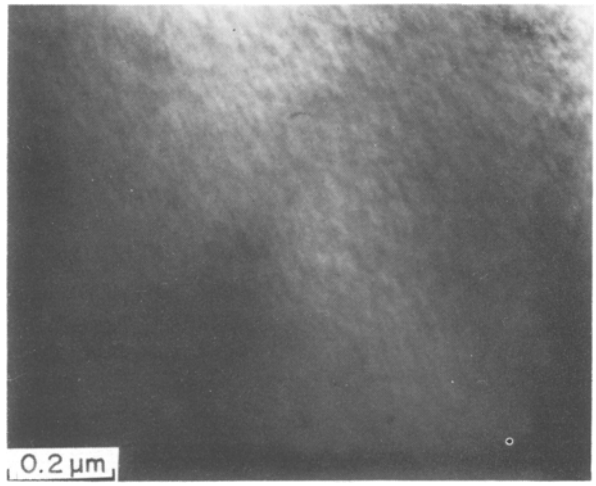

Figure 1 Bright-field electron micrograph of the alloy SA-1 as-quenched from 1323 K.

specimens were aged at temperatues ranging from 723 to 1173 K for suitable durations, in vacuum. Structural changes with ageing were mainly examined by means of transmission electron microscopy (JEM 200A operated at 200 kV). The thin foils for TEM were prepared by electropolishing in an electrolyte of CH_3OH 70% and HNO_3 30% kept at about 200 K.

The electron beam was incident vertically upon a (0 1 1) plane of the thin foil, resulting in simultaneous formations of 2 0 0 and 1 1 1 super reflection spots in one reflection pattern. Since the 2 0 0 spot is induced from both the B2 and DO_3 ordered phases while the 1 1 1 spot comes only from DO_3 ordered phase, these two ordered phases are discriminated by comparison of the 2 0 0 dark-field image with the 1 1 1 dark-field image. The modulated structures in the bright-field images were observed under conditions of $\boldsymbol{g} = 400$. In

TABLE II Microstructure of Fe–Si–Al ternary alloys and of some Fe–Si and Fe–Al binary alloys aged at various temperatures

Alloy	Temperature (K) 723	773	823	873	923	973	1023	1073	1123	1173	ST temperature	Group
S-1				B2			α				α	1
S-2							B2			α	α	
SA-1					B2			α			α	
SA-2		B2 + DO_3					B2		α		α	
SA-3							B2			α	α	
SA-4								B2			B2	
AS-4							B2				(LQ)	
SA-7				B2				α			α	2
SA-8								B2			α	
SA-11								α			α	
SA-12		α + DO_3						B2		No Exam.	α	
SA-13								α			α	
SA-14					B2 + DO_3			B2		α	α	
S-3						DO_3					(LQ)	3
S-4						DO_3					(LQ)	
S-5						DO_3				B2	B2	
S-9						DO_3				B2	B2	
SA-15			DO_3				B2				B2	
AS-1			DO_3				B2				(LQ)	
AS-2			DO_3				B2				(LQ)	
AS-3	DO_3						B2				(LQ)	
AS-5							B2				(LQ)	
A-1	DO_3				B2					No Exam.	(LQ)	
A-2					B2					No Exam.	(LQ)	
A-3				B2						No Exam.	(LQ)	
SA-6	B2					α					(LQ)	
SA-10						α					α	

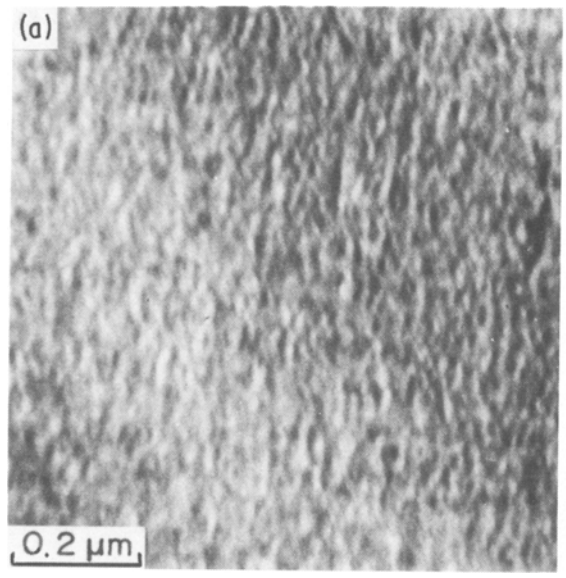

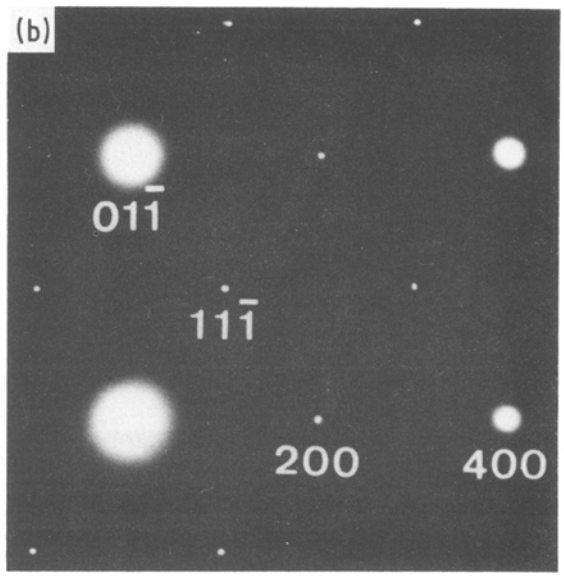

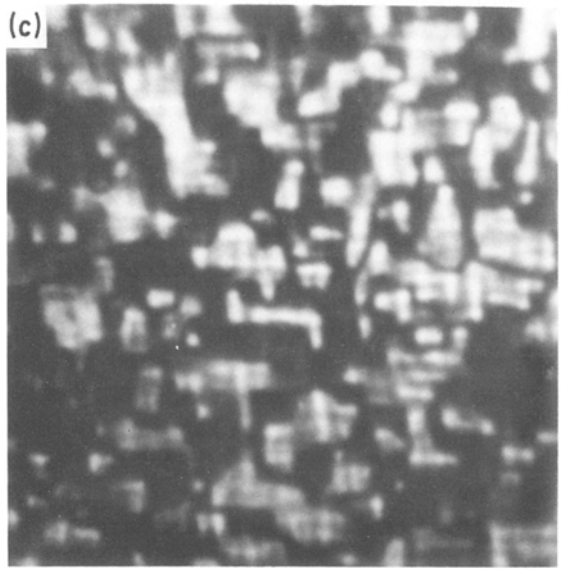

Figure 2 (a) Bright-field image, (b) electron diffraction pattern and (c) dark-field image taken from 2 0 0 super lattice reflection spot, of the alloy SA-1 aged at 823 K for 60 × 10^3 sec.

the present paper the reflection spots are indexed based on a unit cell length of DO_3 lattice, hence the reflection spots of matrix and B2 phases are indexed twice.

3. Experimental results

Structural changes obtained in the present work are summarized in Table II. It is obvious from the table that structural changes with temperature are classified into three groups as shown in Table II. The alloys belonging to the first group have a coexistent region of B2 and DO_3 phases (hereafter represented as B2 + DO_3) at low temperatures and have a B2 single phase region at high temperature. The second group consists of the alloys where the α-Fe + DO_3 region appears at low temperature and B2 or α-Fe phase at high temperature. The third group is those alloys showing no phase separation, i.e. DO_3 single phase at low temperature and B2 phase at high temperature. Details of structural changes for each group are represented below.

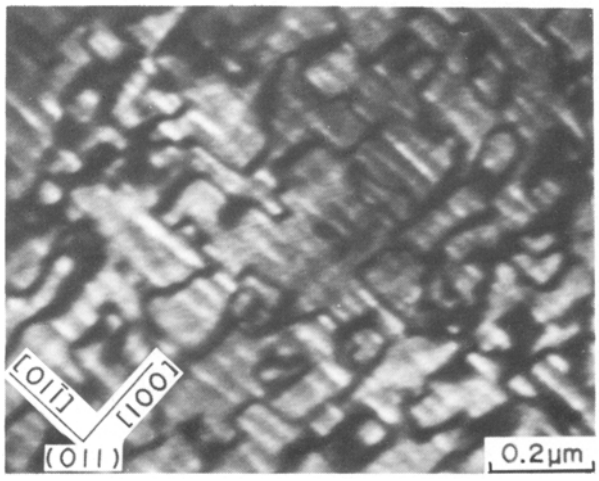

Figure 3 2 0 0 dark-field image of the alloy SA-1 aged at 823 K for 230.4 × 10^3 sec.

3.1. B2 + DO_3 phase-separation (group 1)

Fig. 1 is a transmission electron micrograph of the as-quenched SA-1 ternary alloy whose chemical composition is very close to the Fe–Si binary system, showing no phase decomposition during quenching. Fig. 2a, a bright-field image of the alloy aged for 60 × 10^3 sec at 823 K, shows many wavy striations perpendicular to the [1 0 0] direction. The diffraction pattern (Fig. 2b) clearly shows super lattice reflection spots of 2 0 0 and 1 1 $\bar{1}$. In a dark-field image taken from the 2 0 0 spot (Fig. 2c), many small and bright rod-shaped contrasts can be seen in the ordered regions. These ordered regions grow in size with further ageing.

In Fig. 3 two types of ordered phase are clearly recognized: one is a rod-shaped and brighter phase perpendicular to the [1 0 0] direction and the other is a massive and less bright phase. Figs 4a and b show 2 0 0 and 1 1 1 dark-field images of the alloy, respectively. Since the 2 0 0 super lattice reflection spots arise from both the B2 and DO_3 phases, while the 1 1 1 spot comes only from DO_3 phase, these rod-shaped regions in Fig. 4a are considered to be DO_3 phase and the massive matrix to be B2 phase. Thus, this ordered alloy must be a phase separation of B2 + DO_3. The

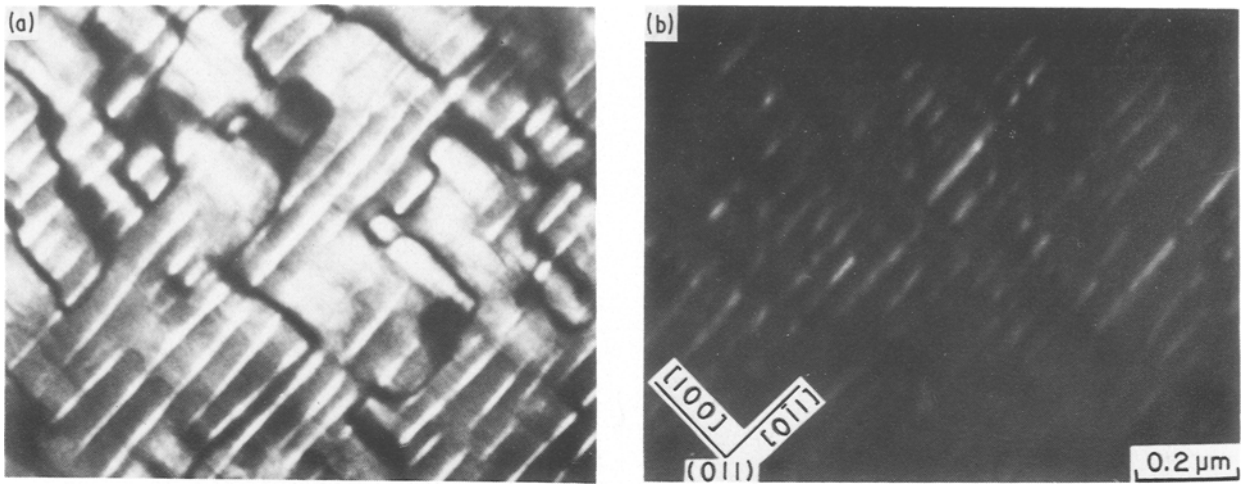

Figure 4 (a) 2 0 0 dark-field image and (b) 1 1 1 dark-field image of the alloy SA-1 aged at 823 K for 921.6 × 10^3 sec, showing B2 + DO_3 phase separation.

brightness of the rod-shaped DO_3 increases with ageing time, which may suggest a progress of ordering of the DO_3 phase. The microstructural changes described above are for the case of 823 K ageing. The same microstructural changes are also observed for other ageing temperatures, such as 723, 773 and 823 K (see Table II).

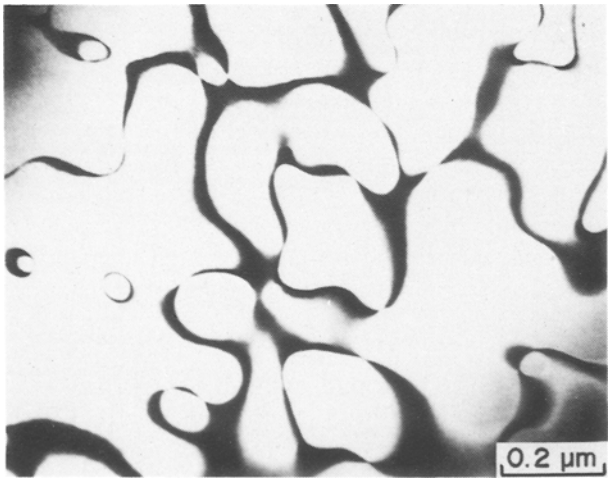

Figure 5 2 0 0 dark-field image of the alloy SA-1 aged at 923 K for 7.2 × 10^3 sec.

If the SA-1 alloy is aged at a higher temperature (923 K), the microstructure, taking on a new turn, shows no phase separation and only anti-phase boundary (APB) of B2, as is represented in Fig. 5. The electron diffraction pattern of this figure showed only the 2 0 0 reflection spots without the 1 1 1 spots coming from the DO_3 phase. Therefore, the SA-1 alloy is sure to be in the B2 single phase region at 923 K. The B2 single region exists in equilibrium up to 1023 K, but at temperatures above 1073 K the α-Fe solid solution is stable.

The phase separation of B2 + DO_3 can also be judged from the age-hardening behaviour of alloys. Fig. 6 shows the age-hardening curves of S-1 alloy where phase decomposition of B2 + DO_3 occurs at temperatures up to 823 K, while at 873 K there is no phase separation, i.e. B2 single phase (see Table II). It is obvious from Fig. 6 that when the alloy is aged at 873 K a primary age-hardening due to B2-ordering is only recognized in the early stage of ageing, while when the alloy is held at the two-phase region (B2 + DO_3) the secondary hardening caused by the phase separation of B2 + DO_3 follows the primary hardening.

The coexistence of B2 + DO_3 is never in a metastable state during transition of a stable single phase

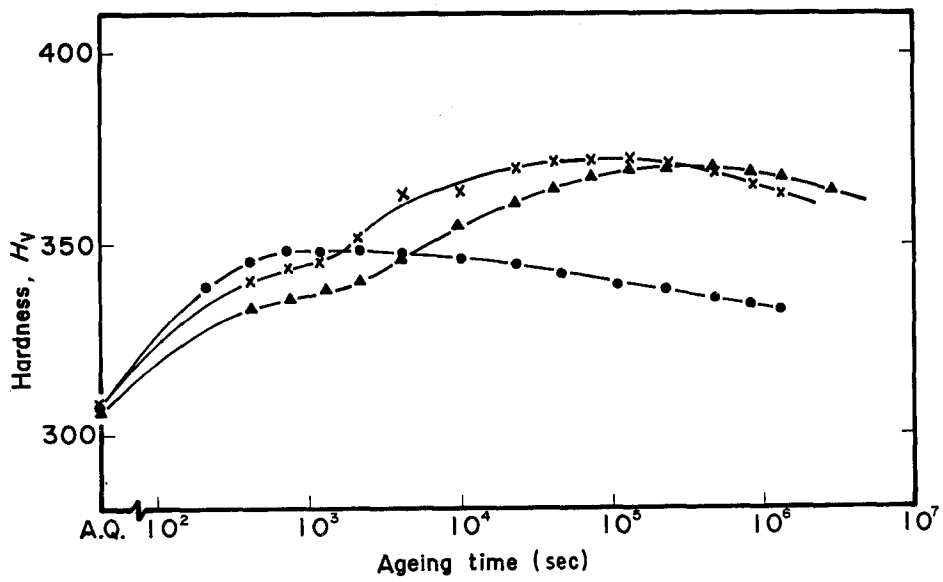

Figure 6 Changes in hardness of the alloy S-1 with ageing at (▲) 773, (x) 823 and (●) 873 K.

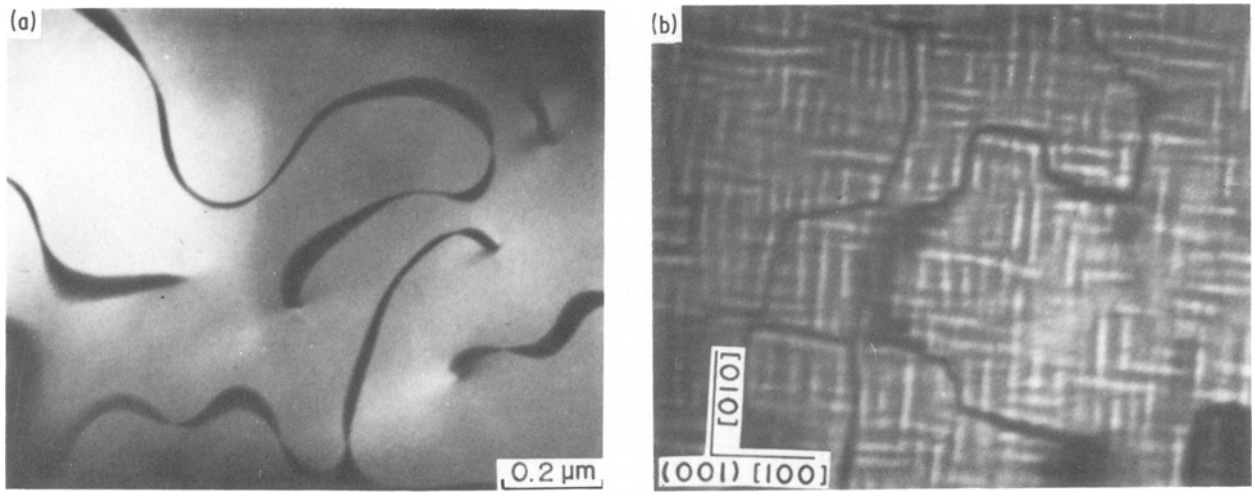

Figure 7 2 0 0 dark-field images of the alloy SA-1 at (a) 923 K for 14.4 × 10^3 sec and (b) 873 K for 230.4 × 10^3 sec after pre-ageing of (a). Reheating of (b) at 923 K produces a microstructure like (a) again.

to another single phase, such as a transition of B2 single phase to DO_3 phase. The two microstructures shown in Figs 7a and b clearly show the structural changes to be reversible, accordingly the coexistence of B2 + DO_3 is sure to be formed in equilibrium through a phase separation provided for the phase diagram.

The microstructural changes described for the SA-1 alloy were also observed in the SA-2, SA-3, AS-4 ternary alloys and in the S-1 and S-2 binary alloys (see Table II). The chemical compositions of these ternary alloys, except the AS-4 alloy, are close to the Fe–Si binary system, hence it is considered that the two-phase region of B2 + DO_3 lies continuously from the Fe–Si binary system into the Fe–Si–Al ternary system. On the other hand, the AS-4 alloy is far apart from these ternary alloys in composition and preferably close to the Fe–Al binary systems. The B2 + DO_3 phase separation has never been observed in the Fe–Al binary system. Therefore, the appearance of B2 + DO_3 in this alloy is remarkable. Figs 8a and b show examples of such B2 + DO_3 microstructure in the AS-4 alloy aged at 773 K.

The morphology of the microstructures shown in Figs 3 and 4 is a modulated structure along the ⟨1 0 0⟩ direction, which differs from the mottled structure of Fe–Al binary alloy, reported by Allen and Cahn [4] and Oki *et al.* [8]. The cause of such morphological variation may result from differences in the compositional expansion coefficient ($\eta = (1/a)\,\partial a/\partial c$) between Fe–Al and Fe–Si binary systems: η is nearly zero at the composition of 20 to 30 at % Al in the Fe–Al system [26], while it is not so small in the Fe–Si alloy, i.e. −0.076 [26].

3.2. α + DO_3 phase-separation (group 2)

Figs 9a, b and c represent microstructures of the SA-7 alloy aged at 823 K for long durations. The bright-field image (a) shows obvious microstructures consisting of two phases. The 2 0 0 dark-field image (b) and the 1 1 1 dark-field image (c) are morphologically identical, which differ from the case of B2 + DO_3 phase separation, and accordingly the bright parts of (b) and (c) are considered to be DO_3 phase, not B2 phase. Therefore, Fig. 9 inevitably results in the coexistent state of the α + DO_3 phases. This type of phase-separation was observed at temperatures below 823 K in this alloy, while at temperatures ranging from 873 to 973 K, the B2 single phase and, above 1023 K, the α-Fe single phase were experimentally observed.

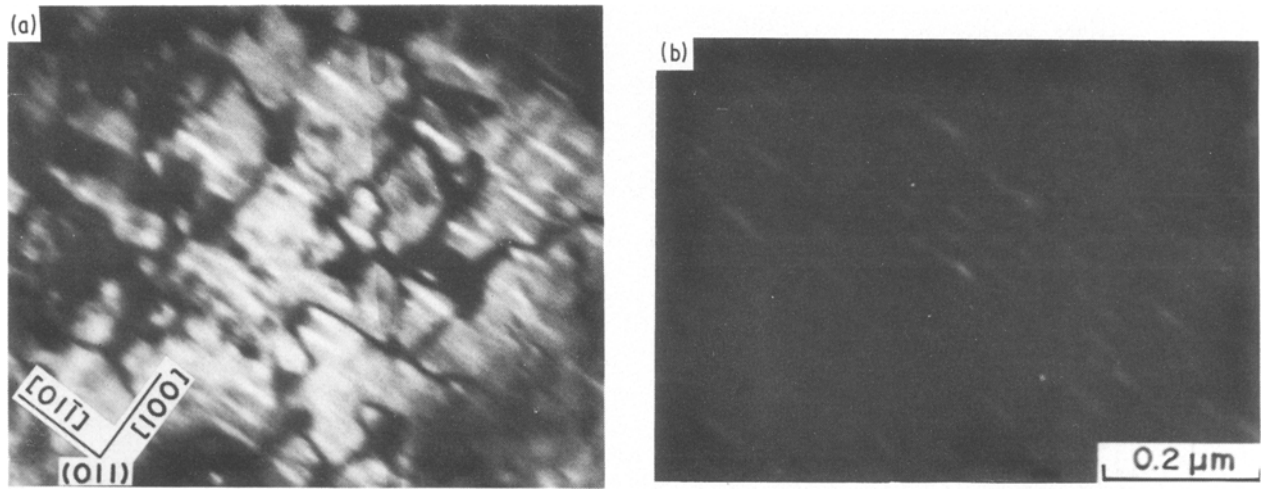

Figure 8 (a) 2 0 0 dark-field image and (b) 1 1 1 dark-field image of the alloy AS-4 aged at 773 K for 604.8 × 10^3 sec.

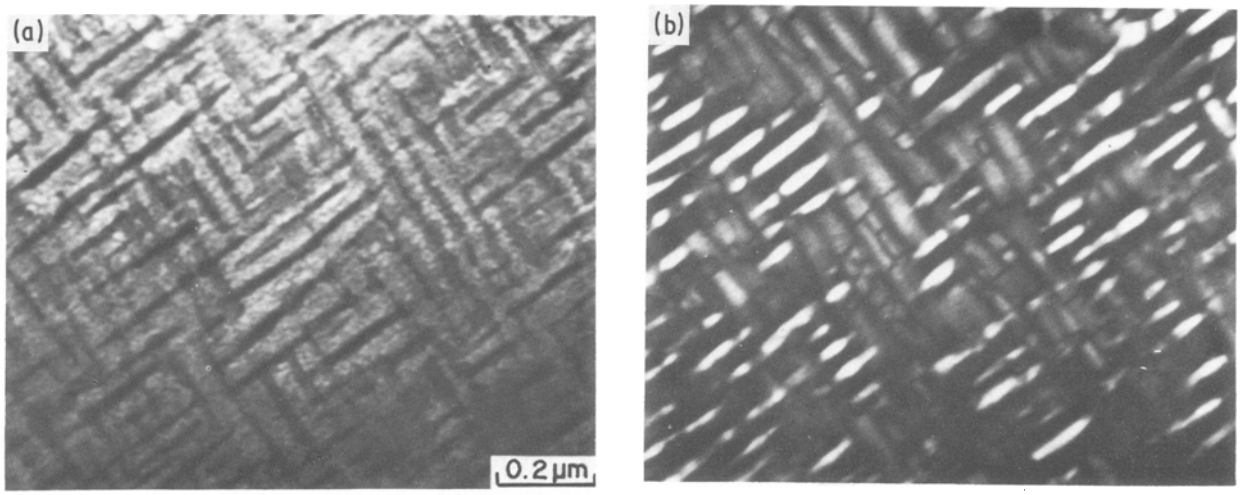

Figure 9 (a) Bright-field image, (b) 200 dark-field image and (c) 111 dark-field image, of the alloy SA-7 aged at 823 K for 921.6×10^3 sec.

The phase separation of $\alpha + DO_3$, although theoretically predicted by Inden and co-workers [14–18] in the Fe–Si binary alloy system, has not been found experimentally in the Fe–Si binary system. By addition of a small amount of aluminium the region of $\alpha + DO_3$ in the Fe–Si binary system may rise to a temperature high enough for atom-diffusion to occur. The $\alpha + DO_3$ phase separation is also observed in SA-11 alloy whose composition is close to the Fe–Al binary system as represented in Fig. 10. From Figs 9 and 10, the $\alpha + DO_3$ phase separation is considered to lie in a narrow band region connecting the Fe–Si and Fe–Al binary systems.

Most of the alloys decomposing to $\alpha + DO_3$ at low temperature have a B2 single phase region at higher temperatures, but in the SA-14 alloy, the B2 + DO_3 region exists on the high temperature side of the region of $\alpha + DO_3$. Fig. 11 shows such a B2 + DO_3 phase separation in the SA-14 alloy. The B2 + DO_3 region in this alloy was only observed at temperatures of 913 and 923 K, while at 898 K the $\alpha + DO_3$ phase separation and at 938 K the B2 single phase were experimentally obtained. Therefore, the B2 + DO_3 region of SA-14 alloy is in a very narrow temperature range.

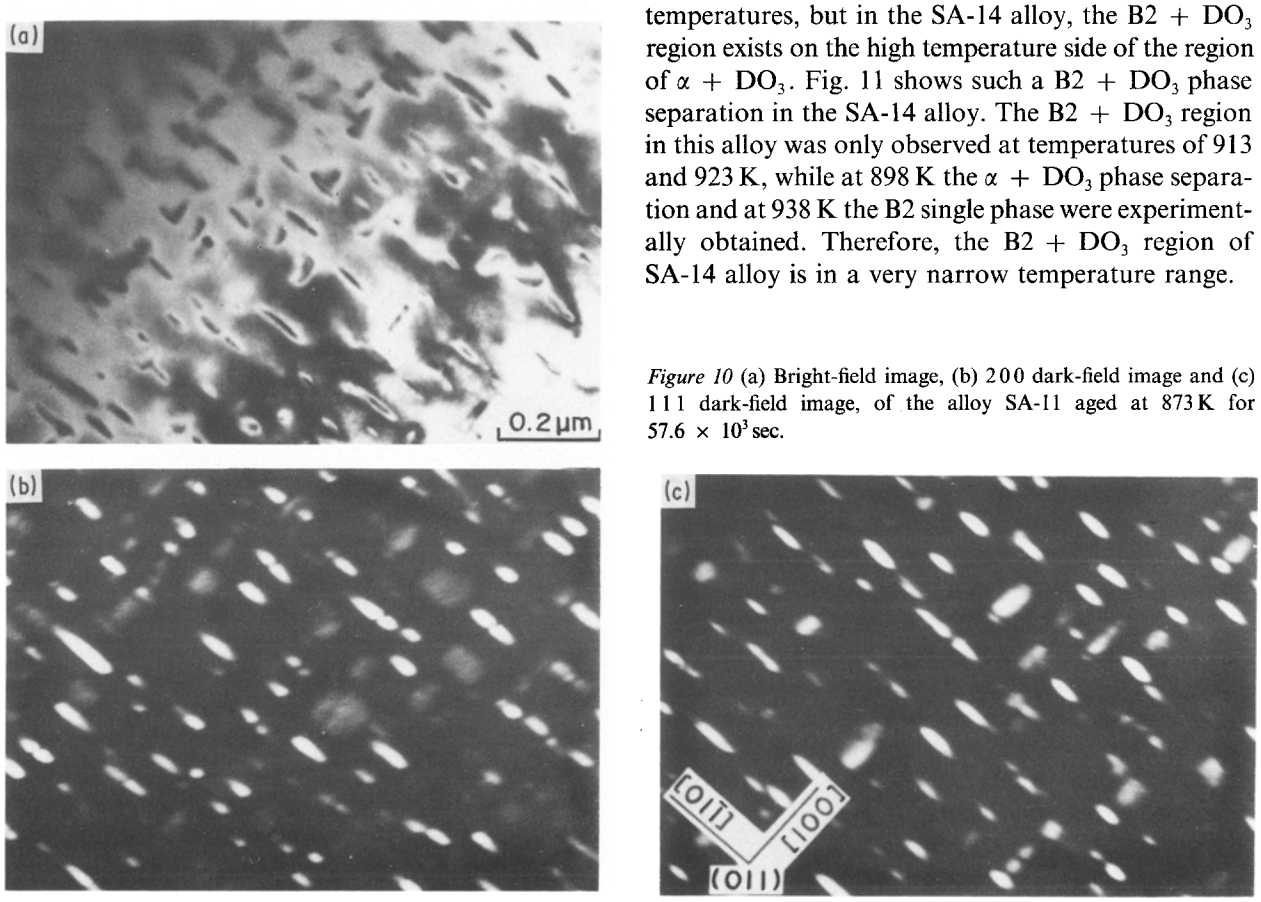

Figure 10 (a) Bright-field image, (b) 200 dark-field image and (c) 111 dark-field image, of the alloy SA-11 aged at 873 K for 57.6×10^3 sec.

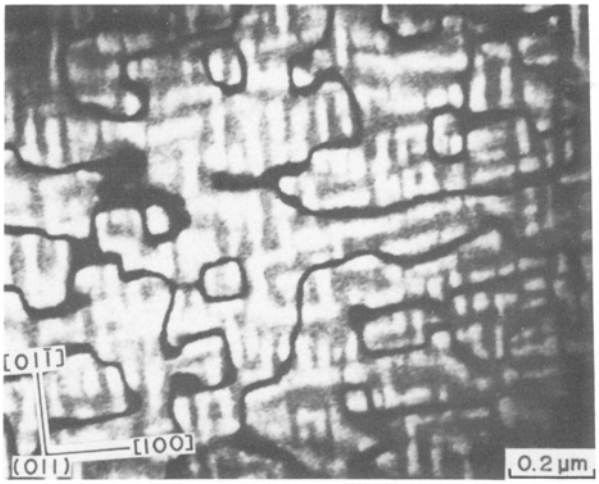

Figure 11 2 0 0 dark-field image of the alloy SA-14 aged at 923 K for 3.6×10^3 sec.

3.3. No phase-separation (group 3)

Fig. 12 is a dark-field image taken from the 1 1 1 reflection spot of the SA-15 alloy aged at 873 K, showing clearly that the alloy was held in the DO_3 single phase. When the alloy was held at higher temperatures (above 973 K), the 1 1 1 reflection spot disappeared and only the 2 0 0 reflection spot remained, which indicates a phase transition of DO_3 to B2 without phase separation. Such a single phase transition was observed in many alloys shown in Table II.

3.4. Phase diagrams

On the basis of the many microstructural examinations, the phase diagrams of the Fe–Si–Al ternary system at various temperatures are represented in Figs 13 and 14.

One essential difference in the phase diagrams of Fe–Si and Fe–Al binary systems is the stability of the DO_3 phase: the DO_3 phase is more stable in the Fe–Si systems, as is seen in Fig. 13. Thereby, generally the lower temperature part of the Fe–Si phase diagram corresponds to the higher temperature part of the Fe–Al system. Therefore, in the isothermal section diagrams of the Fe–Si–Al ternary system, the phase changes from the higher temperature part to the lower temperature part of the Fe–Si alloy appear as the composition shifts from the Fe–Si binary side to the Fe–Al side in the ternary system, i.e. the B2 + DO_3 two phase region moves to the α + DO_3 region.

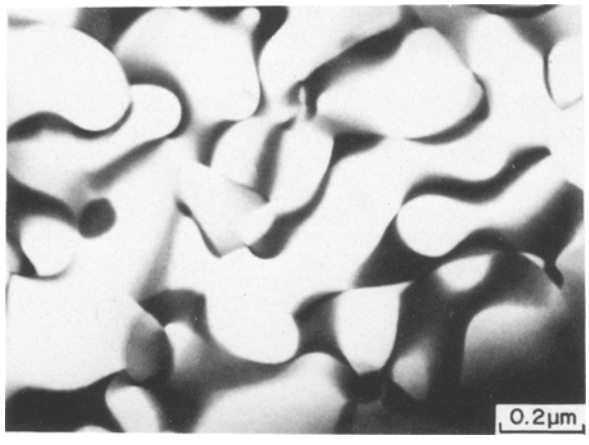

Figure 12 1 1 1 dark-field image of the alloy SA-15 aged at 873 K for 7.2×10^3 sec.

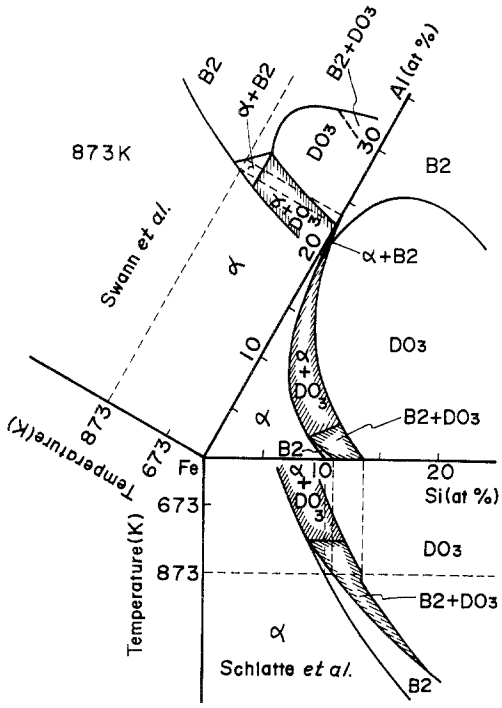

Figure 13 An isothermal section diagram at 873 K of the Fe–Si–Al ternary alloy and phase diagrams of Fe–Si and Fe–Al binary systems.

4. Conclusion

Stable structures of Fe–Si–Al ternary alloys and Fe–Si and Fe–Al binary alloys containing up to about 40 at % solute atoms were investigated by means of transmission electron microscopy. The results obtained are as follows. Two types of phase separation, B2 + DO_3 and α + DO_3 are observed in the alloys whose compositions lie in a narrow band connecting Fe–10 to 14 at % Si with Fe–20 to 25 at % Al and also in the neighbourhood of a Fe–30 at % Al–3 at % Si alloy. Such compositions of the alloys are located in the phase boundary of B2 and DO_3 single phases or α and DO_3 single phases. The phase separation in the Fe–Si–Al and Fe–Si alloys produce the ⟨1 0 0⟩ modulated structure which differs from the morphology formed by the phase separation of the Fe–Al system.

Acknowledgement

This work was supported in part by a Grant-in-Aid for Scientific Research from Ministry of Education, Japan.

References

1. M. BOUCHARD and G. THOMAS, *Acta Metall.* **23** (1975) 1485.
2. H. KUBO and C. M. WAYMAN, *Met. Trans.* **10A** (1979) 633.
3. H. KUBO, I. CORNEILS and C. M. WAYMAN, *Acta Metall.* **22** (1974) 201.
4. S. M. ALLEN and J. W. CAHN, *ibid.* **23** (1975) 1017.
5. S. M. ALLEN, *Phil. Mag.* **36** (1977) 181.
6. P. R. SWANN, W. R. DUFF and R. M. FISHER, *Trans. Met. Soc. AIME* **425** (1969) 851.
7. *Idem, Met. Trans.* **3** (1972) 409.
8. K. OKI, H. SAGANE and T. EGUCHI, *Jpn. J. Appl.*

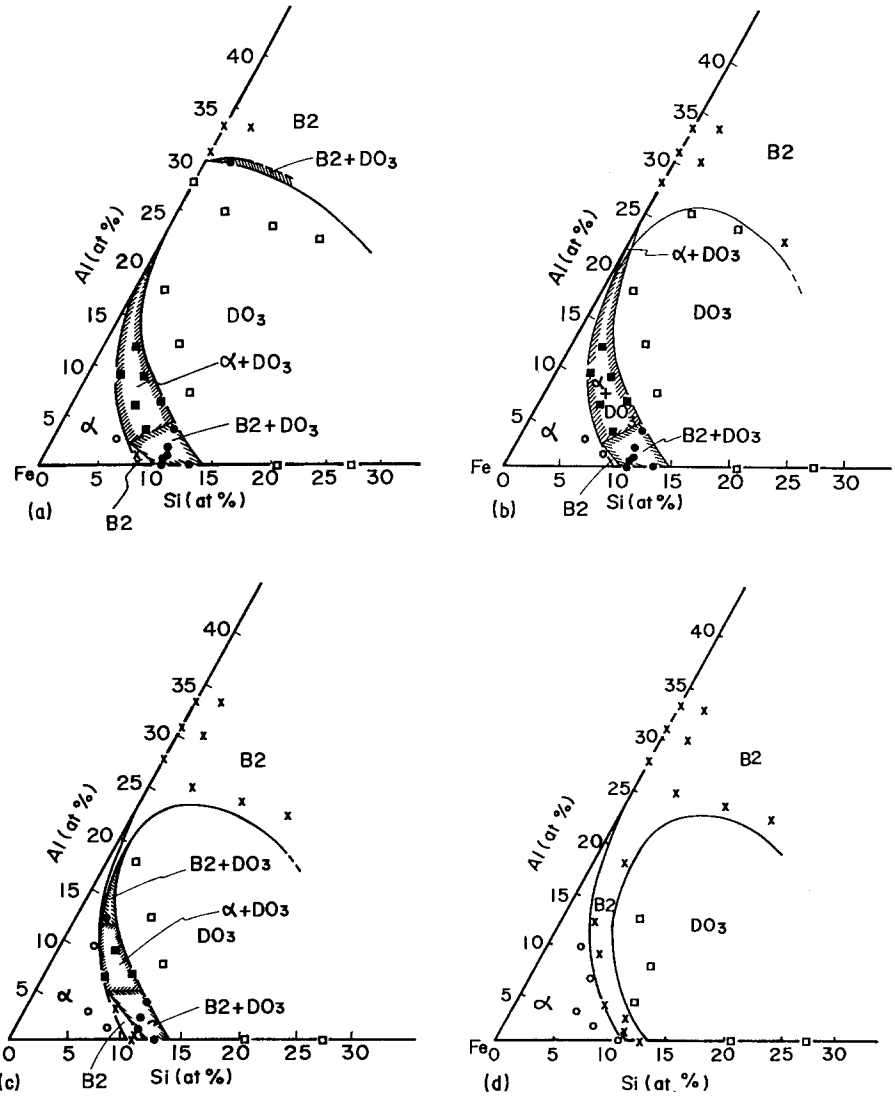

Figure 14 Isothermal section diagrams of the Fe–Se–Al ternary alloy systems at (a) 723 K, (b) 823 K, (c) 923 K and (d) 973 K. ○, α-phase; x, B2 phase; □, DO_3 phase; ●, B2 + DO_3 phases; ■, α + DO_3 phases.

Phys. **13** (1974) 753.

9. H. SAGANE, K. OKI and T. EGUCHI, *Trans. Jpn. Inst. Metals* **18** (1977) 48.
10. G. INDEN and W. PITSCH, *Z. Metallkde* **63** (1972) 253.
11. H. H. ETTWIG and W. PEPPERHOFF, *ibid.* **63** (1972) 453.
12. G. SCHLATTE and W. PITSCH, *ibid.* **66** (1975) 660.
13. P. R. SWANN, L. GRANAS and B. LEHTINEN, *Met. Sci.* **9** (1975) 90.
14. G. INDEN, *Z. Metallkde.* **66** (1975) 577.
15. *Idem, ibid.* **66** (1975) 648.
16. *Idem, ibid.* **68** (1977) 529.
17. G. INDEN and W. PITSCH, *ibid.* **62** (1971) 627.
18. G. SCHLATTE, G. INDEN and W. PITSCH, *ibid.* **65** (1974) 94.
19. V. PAIDER, *Phys. Status Solidi* (*a*) **21** (1974) K73.
20. H. WARLIMONT, *Z. Metallkde* **59** (1968) 595.
21. H. KUBO, *J. Phys. Chem. Solids* **44** (1983) 323.
22. D. de FONTAINE, "Solid State Physics", Vol. 34 (Academic Press, 1979) p. 73.
23. S. M. ALLEN and J. W. CAHN, *Acta Metall.* **24** (1976) 425.
24. M. HASAKA and S. IKEDA, *J. Jpn. Inst. Metals* **44** (1980) 180 (in Japanese).
25. N. TSUYA and K. I. ARAI, *J. Appl. Phys.* **50** (1979) 1658.
26. W. B. PEARSON, "A Handbook of Lattice Spacings and Structures of Metals and Alloys" (Pergamon, 1959).

Received 23 August
and accepted 4 October 1985